PeerJ Preprints NOT PEER-REVIEWED

The Investigation of Metal-ion Coordination to Amyloid-Beta and Potential Chelation Materials for the Treatment of Alzheimer's Disease

Neha Pavuluru[1] **and Xuan Luo**[2]

[1]**National Graphene Research and Development Center, Springfield, Virginia 22151, USA**
[2]**National Graphene Research and Development Center, Springfield, Virginia 22151, USA**

Corresponding author:
Xuan Luo[1]

Email address: xuan.us@gmail.com

ABSTRACT

Alzheimer's disease is a neurodegenerative disorder that results in the death of neurons and impaired cognitive function. One of the pathological hallmarks of Alzheimer's is the formation of senile plaques which originate from the aggregation of the Amyloid-β protein. Recent research has found that the overabundance of certain metal-ions in the brain may contribute to this problem, and that chelation therapy may be an effective tool to solve it. In this study, we conducted Density Functional Theory calculations to investigate the interaction of metal ions to the Amyloid-β protein, as well as the adsorption of the copper-ion by potential chelation materials. We conducted binding energy calculations and plotted the charge transfer between the metals and the substrates in order to evaluate bond strength. Binding energy calculations revealed that the binding affinities followed the order of Cu $>$ Al $>$ Zn, proving copper to retain the strongest affinity compared to other metal ions of biological significance. Due to copper's strong affinity, binding energies were also evaluated for its interaction with potential chelators: monolayer boron nitride, monolayer molybdenum disulfide, and monolayer silicene. Silicene produced the highest binding energies to copper, and the evidence of charge transfer between copper and the monolayers proves that there is a strong ionic bond present. Although our three monolayers did not directly present chelation potential, the absolute differences between the binding energies of the silicene binding sites and the Amyloid-β binding sites were minimal proving that further research in silicene chelators will open doors for therapy in Alzheimer's disease.

INTRODUCTION

Alzheimer's disease (AD) is the most common cause of dementia worldwide, with a growing prevalence in older individuals (Hardy and Higgins (1992)). AD is a neurodegenerative disease that interferes with the synaptic responses in the brain leading to the death of neurons (DeKosky and Scheff (1990)). The continuous deterioration of neurons leads to impaired cognitive function and behavior in AD patients, placing a significant socioeconomic toll on both the individual and family members (Selkoe (2001); Riley et al. (2002)). These degenerative changes are frequently attributed to neurofibrillary tangles and tau hyperphosphorylation, two pathological hallmarks of AD (Cheng et al. (2006)). However, the main antagonists in AD are understood to be senile plaques (Hardy and Higgins (1992); Dickson et al. (1988)).

Senile plaques are a result of Amyloid-Beta (Aβ) protein aggregation (Pappolla et al. (1998)). Aβ is a 40-42 amino acid residue peptide cut from the C terminal of the amyloid precursor protein (APP) (Pappolla et al. (1998); Tanzi et al. (1987); Lesné et al. (2006)). When cut from the β- and γ-secretases, Aβ misfolds and aggregates into senile plaques (Lesné et al. (2006); Smith et al. (2007)). An area of interest in Aβ research is the hypothesis that metal ions interact with segments of Aβ and accelerate its aggregation into senile plaques (Lee et al. (2018); Barnham and Bush (2014)). These metal ions interface

with the protein by strengthening the formation of beta pleats (Viles (2012)), as well as by strengthening the hydrophilic interactions between certain amino acids, such as His and Asp, by forming salt bridges (Faller et al. (2013)). Both actions are crucial to the development of Aβ as salt bridges impact the tertiary structure of the protein while beta pleats impact the secondary structure. Previous in-vitro studies have verified this hypothesis by attributing elevated levels of copper, zinc, and iron to increased Aβ aggregation (Barnham et al. (2007); Tõugu et al. (2011)). Although some studies indicate that metal ions play a role in the formation of senile plaques, uncertainties about the presence of metal ions in Aβ aggregation exist and the mechanisms of metal and Aβ interaction remain unclear. To resolve this ambiguity, recent research efforts have emphasized determining the metal-Aβ binding sites by identifying the coordination point at which the metal ion binds to the amino acid residues (Talley et al. (2002)). Researchers have developed at least three investigational approaches: 1) absorption spectroscopy computational methods; 2), x-ray methods; and first-principles computations (Strodel and Coskuner-Weber (2019)).

Conclusions that were drawn regarding copper coordination to Aβ reveal that it occurs in the Histidine (His) 13 and 14 residues through their nitrogen atoms (Minicozzi et al. (2008b); Curtain et al. (2001); Mutter et al. (2018)) and N-terminal (Hane et al. (2013); Syme et al. (2004); Azimi and Rauk (2011)) along with contribution of one oxygen atom (Rimola et al. (2011)). Zinc coordination is predicted to consist of purely His residues, whereas aluminum requires interaction with oxygen-containing residues. There are several hypotheses regarding metals' structural relationships to Aβ, inconsistencies exist among the varying propositions. For instance, while some studies support tyrosine involvement in copper coordination through its oxygen atom (Minicozzi et al. (2008a)), other works suggest its irrelevance (Minicozzi et al. (2008a); Kowalik-Jankowska et al. (2003); Karr and Szalai (2007)). Contradicting theories also exist in regards to the coordination sequence between copper and regions among the Aβ peptide. Proposed coordinations include four nitrogen (N4), three nitrogen one oxygen (N3O1), and three nitrogen three oxygen (N3O3) patterns (Rauk (2009)).

The role of metal ions in enhancing Aβ aggregation has also led to the possibility of utilizing them as therapeutic targets to halt the progression of AD (Liu et al. (2009)). One proposal to combat metal-induced aggregation is chelation therapy. Chelation is the practice of utilizing certain compounds to remove excess metals in the body. Metal chelates such as clioquinol and PBT2 were found to be effective in clinical trials of brain diseases, such as AD and Huntington's Disease (Ritchie et al. (2003); Lannfelt et al. (2008)), indicating chelation therapy's potential treatment as a treatment for AD. This has encouraged continued development of derivatives to improve clinical effectiveness and reduce cytotoxic effects. However, these previously explored chelation agents are not suitable for treating AD due to their inability to permeate the blood brain barrier, demonstrate efficient selective targeting, and produce tolerable side effects (Minicozzi et al. (2008a)). To overcome the issues of these metal chelates, recent research has encouraged the use of 2D monolayers as therapeutic agents for AD, given the ability of their small size will be able to permeate the blood brain barrier, as well as their superior surface area which would be effective for adsorption. However, the concept of utilizing 2D monolayers in treating AD is relatively new. While research in the field of 2D monolayer chelation is sparse, there have been studies where nanoparticles were utilized for drug-delivery and blood-brain-barrier permeation. These nanoparticles have demonstrated promising results when in previous in-vitro studies. For example, both boron nitride nanotubes and molybdenum disulfide nanoparticles have been used in the treatment of brain diseases (Ciofani et al. (2011); Han et al. (2017)), and recent clinical trials have also found that silica based materials may reduce cognitive impairment associated with AD (Davenward et al. (2013)). Based on this information, we selected three biocompatible monolayers and tested their chelation potential.

In order to make accurate predictions about the interactions between metal ions, 2D nanomaterials, and amino acids, computational platforms, such as theoretical quantum biological and quantum chemical studies, are important in this field (Gomez-Castro et al. (2014); Marino et al. (2010); Drew et al. (2009); Mantsyzov et al. (2018)). One of the important concepts in these calculations is binding energy. Binding energy evaluated from total energy calculations can be used to identify structural relationships between metal ions and Aβ as well as the efficiency of potential chelation treatments. This study will focus on the interactions between the zinc, copper, and aluminum metals and their interactions with the His amino acid residue along with boron nitride, molybdenum disulfide, and silicene. Analysis of these effects are vital towards mitigation of AD as well as exploration of new methods of disease treatment. In this study, we report the specific computational methods used, our results, and direct interpretations of the calculations. We also discuss our findings, as well as the future work to be completed in order to supplement our

findings.

METHOD

0.1 Computational Theory

In this study, we performed Density Functional Theory (DFT) calculations with the Generalized Gradient Approximation (GGA) (Blöchl (1994)) pseudopotentials in the form of Perdew-Burke-Ernzerhof (PBE) (Perdew et al. (1996)) implemented in the ABINIT (Gonze et al. (2009)) code. We used the Projected Augmented Wave (PAW) method to generate the pseudopotentials used. The electron configurations and the radius cutoffs used to generate these PAW pseudpotentials are listed in Table I.

Table 1. *Electron Configurations and Radius Cutoff of Each Element for Generating the PAW Pseudopotentials Used in the Current Study*

Element	Electron Configurations	Radius Cut-Off (Bohr)
Zinc (Zn)	[Ar] $4s^2\ 3d^{10}$	2.31
Aluminum (Al)	[Ne] $3s^2\ 3p^1$	1.90
Copper (Cu)	[Ne] $3s^2\ 3p^6\ 4s^1\ 3d^{10}$	2.02
Boron (B)	[He] $2s^2\ 2p^1$	1.70
Nitrogen (N)	[He] $2s^2\ 2p^3$	1.20
Carbon (C)	[He] $2s^2\ 2p^2$	1.51
Oxygen (O)	[He] $2s^2\ 2p^4$	1.41
Hydrogen (H)	$1s^1$	1.00
Molybdenum (Mo)	[Kr] $4d^5\ 5s^1$	2.20
Sulfur (S)	[Ne] $3s^2\ 3p^4$	1.92
Silicon (Si)	[Ne] $3s^2\ 3p^2$	1.91

0.2 Convergence Calculations

The main calculation that will be conducted in this study is binding energy. In order to find the binding energy, however, the total energy of the materials must be known. Total energy can be determined from a series of calculations which involve finding the kinetic energy cutoff, the K-Mesh, the optimized lattice parameters, and the vacuum height. For both metals and 2D materials, convergence calculations were accomplished using the self-consistent field method. Values were converged until the difference in total forces for two consecutive datasets was less than 1×10^{-4} Ha/Bohr. Lattice parameter relaxation was done using the Broyden-Fletcher-Goldfarb-Shanno (BFGS) method in order to find the optimized lattice parameters. These calculations continued until the maximum forces converged to less than 5×10^{-4} Ha/Bohr. Using these converged values, the total energy can be found. The total energy calculations were carried out using the converged parameters until the difference in total energy in the self-consistent field cycles was less than 1×10^{-10} Ha/Bohr.

0.3 Materials

0.3.1 Pristine Metal and 2D Monolayer Calculations

Convergence of kinetic energy cut-off was calculated for the individual metal ions investigated in this work. This was accomplished using the convergence calculations described above. The metals investigated include copper, aluminum, and zinc and their kinetic energy cutoffs (Ha) are 22, 23, and 20, respectively.

The 2D materials analyzed in this work include boron nitride, molybdenum disulfide, and silicene. Convergence studies were performed for kinetic energy cutoff, vacuum space, and K-Mesh. Converged values were then utilized for relaxation of the atomic structure and unit cell dimensions. These calculations were performed using the 1×1 unit cell. The converged values are presented in Table II.

0.3.2 Metal Interaction with Aβ

Aβ calculations were carried out in both high-pH and low-pH environments to account for Aβ flexibility in different conditions. While both are characterized by an N3O1 sequence, the low-pH binding site consisted of His6, His13/His14, NH_2 of the N-terminal, and an oxygen atom whereas the high-pH components consisted of His6, His13, His14, and Ala2. Ambiguous sequences beyond the direct binding

Table 2. *Converged Kinetic Energy Cut-Off, k-mesh, and vacuum of 2D materials*

Material	Kinetic Energy Cutoff (Ha)	K-Mesh	Vacuum (Bohr)
Boron Nitride	24	6×6×1	13
Silicene	13	12×12×1	18
Molybdenum Disulfide	20	10×10×1	30

at the first coordination sphere were saturated with hydrogen atoms. For accommodation of computational limitations, histidine ligands were modeled by their 4-methylimidazole ($C_3H_4N_2$) side chains, the N-terminal by NH_2 , and the alanine side chain was modelled by an OH group. The metal ions investigated within developed structures at the central location were Cu, Zn, and Al.

Initial first coordination sphere complexes were constructed and optimized in the Jmol software. The corresponding coordinates of the complexes of the structure were then exported and used in optimization calculations. The complex was relaxed, and optimized geometries were used to calculate the total energy of the complex, both with and without coordination to metal ion.

Total energy calculations were then run for successful configurations: for the total interface, the isolated metal molecule, and the isolated surface. Binding energy was defined by

$$E_{binding} = E_{substrate+metal} - E_{metal} - E_{substrate} \quad (1)$$

where $E_{binding}$ represents the binding energy, $E_{metal+substrate}$ is the total energy of the metal-substrate complex, $E_{substrate}$ is the total energy of the substrate, and E_{metal} is the total energy of the individual metal ion. Higher magnitudes are associated with higher affinities.

0.3.3 Metal Interaction with 2D Monolayers

Metal interactions with 2D materials were accomplished using a 2×2 supercell. The vacuum was the same as that converged using the 1×1 unit cell. Out of the determined kinetic energy cutoffs of the metals and the 2D materials, the higher kinetic energy cutoff was chosen for the 2×2 supercell. The k-mesh was halved, and the unit cell dimension doubled. Metal-ion coordination was observed at three binding locations to determine the most optimal binding site. The binding locations consisted of the top of the atoms, the hollow of the surface, and the bridge site. Total energy calculations were carried out for the individual metal-ions, the 2D material, and the metal-2D complex. Potential chelation candidates were determined by comparing the binding energies of the metal-ions and 2D materials to the binding energies of the metal-ions and the Aβ structure.

Furthermore, charge density values were evaluted by using this equation

$$\Delta\rho = \rho_{metal+substrate} - \rho_{metal} - \rho_{substrate} \quad (2)$$

where $\Delta\rho$ represents the charge transfer between the metal and the substrate, $\rho_{metal+substrate}$ represents the charge of the metal-substrate complex, ρ_{metal} represents the charge of the individual metal ion, $\rho_{substrate}$ is charge of the individual substrate. Isosurface values were determined to display the charge densities at select viewing sites.

1 RESULTS

In this section, we report our results on the binding strength between the selected metals and substrates (Aβ and 2D monolayers). Referring to Equation 1, binding energies were calculated through relating the total energies of the metal, the substrate, and the metal-substrate complex. These binding energies were used to further analyze and interpret the meaning of our results in the context of the issue, or specifically, the chelation potential of the explored treatment materials. Charge transfer was also plotted using Equation 2 to determine the strengths of the bonds between copper and the monolayers.

1.1 Pristine Metals and 2D Monolayers

The optimized lattice parameters calculated in this study as well as the experimental lattice parameters from previous studies are listed in Table III and the visualizations of the 2D Monolayers can be seen in

Figure 1. Based on the table, we can see that the lattice parameters obtained in this study closely resemble the experimental values.

Table 3. *Optimized Lattice Parameters and Experimental Lattice Parameters of the Bulk Metals and Pristine 2D Monolayers*

Material	Current Calculation (Bohr)	Experimental Calculation (Bohr)	% Error
Copper	6.74	6.79Davey (1925)	0.7364
Zinc	5.16	5.03Datta et al. (2006)	2.5845
Aluminum	7.65	7.65Davey (1925)	0
Boron Nitride	4.75	4.73Wang et al. (2017)	0.4228
Molybdenum Disulfide	5.98	5.91Molina-Sanchez and Wirtz (2011)	0.4228
Silicene	7.23	7.29Pflugradt et al. (2014)	0.8230

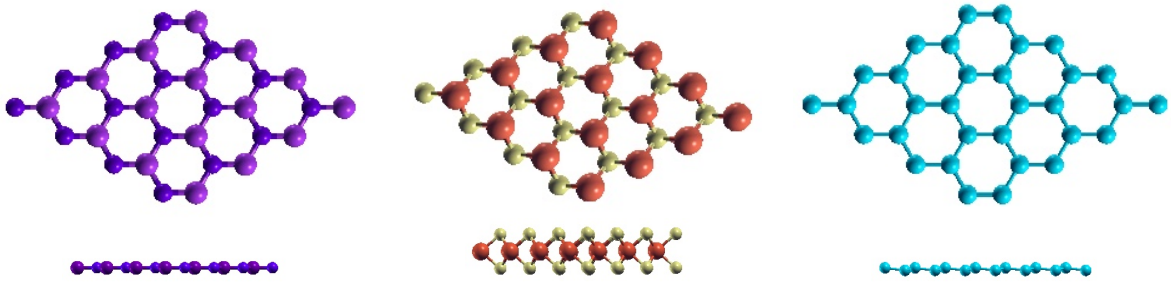

(a) (b) (c)

Figure 1. *The visualizations of the top and side views of the relaxed monolayers (a) boron nitride, (b) molybdenum disulfide, (c) silicene. In these structures, boron is represented by purple, nitrogen by dark blue, sulfur by yellow, molybdenum by orange, and silicon by light blue.*

1.2 Metal Interaction with Aβ

Metal-ion and Aβ calculations were carried out using the N3O1 sequence of the Aβ first-coordination sphere in the high-pH and the low-pH environments. The high-pH coordination sphere consisted of 3 His ligands and oxygen atom, whereas the low-pH coordination sphere contained 2 His ligands, an NH_2 group, and an OH group. Relaxation calculations were done for the complex in a large box and the optimized lattice parameters and atomic coordinates were used to find the total energies.

The optimized geometries of metal ion coordination to the low-pH coordination sphere are visualized in Figure 2, the high-pH visualizations are seen in Figure 3, and the binding energies are presented in Table IV.

Table 4. *Binding energies for the low-pH and high-pH Aβ metal-ion complexes*

Element	E_{low-pH} (Ha)	$E_{high-pH}$ (Ha)
Copper	-0.6842	-0.7262
Zinc	-0.0251	-0.0925
Aluminum	-0.4230	-0.4780

The described results derived from total energy calculations reveal that the first coordination sphere of Aβ exhibits the strongest affinity for copper in a low-pH environment, whereas zinc exhibits the weakest affinity. We also calculated the bond lengths of the metal-Aβ complex in the low-pH environment. Unrelaxed, the bond lengths between the metal and the nitrogen of the first His ligand, the metal and the nitrogen of the second His ligand, and the metal and the oxygen atom of the OH group were 2.78 Bohr, 4.27 Bohr, and 3.27 Bohr , respectively. After relaxation, the bond length between copper and the N atom of the first His ligand as well as copper and the oxygen atom of the OH group increased, whereas the

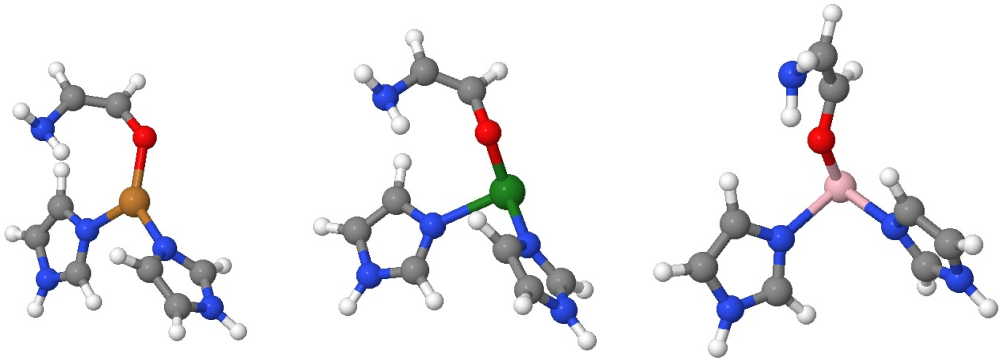

(a) (b) (c)

Figure 2. *Fully relaxed metal-ion and low-pH Aβ complexes. (a) copper-Aβ, (b) zinc-Aβ, and (c) aluminum-Aβ. For the Aβ ligands, carbon is represented by grey, hydrogen by white, nitrogen by blue, and oxygen by red. For the metals at the center of these structures, copper is represented by brown, zinc by green, and aluminum by pink*

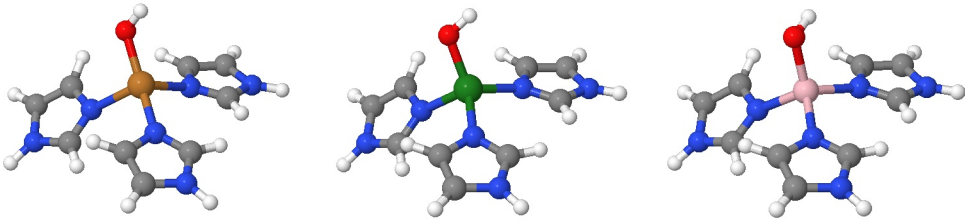

(a) (b) (c)

Figure 3. *Fully relaxed metal-ion and high-pH Aβ complexes. (a) copper-Aβ, (b) zinc-Aβ, and (c) aluminum-Aβ. For the Aβ ligands, carbon is represented by grey, hydrogen by white, nitrogen by blue, and oxygen by red. For the metals at the center of these structures, copper is represented by brown, zinc by green, and aluminum by pink*

bond length of copper and the N atom of the second His ligand decreased. The resulting values were 3.84 Bohr, 3.55 Bohr, and 3.63 Bohr , respectively. We also examined the bond lengths between zinc and Aβ after relaxation. We found that, similar to copper, bond lengths between the N atom of the first His ligand the oxygen atom of the OH group increased, whereas the bond length between the N atom of the second His ligand decreased. The obtained values were 4.18 Bohr, 3.67 Bohr, and 4.12 Bohr , respectively. Although the changes in bond lengths indicated structural diffrences for each of the metal-Aβ complexes, significant changes were not observed. Lack of structural changes reveal that the complex stayed intact and withstood dissociation.

Analogous to the total energy calculations done on the low-pH Aβ and metal-ion complexes, we found that copper exhibited the highest binding affinity towards the Aβ protein in a high-pH environment as well, whereas zinc exhibited the lowest binding affinity. Unlike the low-pH environment, however, the high-pH environment produced higher binding energies for all three of the metal-Aβ complexes. We also calculated the bond lengths of the metal-Aβ complex in the high-pH environment. Before relaxation, the bond lengths of the metal and the nitrogen of the first His ligand, the metal and the nitrogen of the second His ligand, the metal and the nitrogen of the third His ligand, and the metal and the oxygen atom were 3.65 Bohr, 3.55 Bohr, 3.51 Bohr, and 3.29 Bohr , respectively. After relaxation, the bond length between copper and all four atoms increased. The resulting values were 4.25 Bohr, 3.63 Bohr, 4.38 Bohr, and 3.53 Bohr , respectively. We also examined the bond lengths between zinc and Aβ after relaxation. We found that, similar to copper, all of the bond lengths had increased. The obtained values were 3.95 Bohr, 3.89 Bohr, 3.93 Bohr, and 3.53 Bohr , following the same order as copper-Aβ. Similar to the low-pH complexes, the metal-Aβ complex in a high-pH environment underwent minor structural changes,

however, nothing significant was observed.

1.3 Metal Interaction with 2D Monolayers

Because of copper's high affinity towards both the low-pH and high-pH structures of the Aβ protein, we proceeded to investigate its attraction towards the different 2D monolayers. Total energy investigations of atom absorption to boron nitride, MoS_2, and silicene along with calculated binding energies are presented in Table V, VI, and VII, respectively. Based on Equation 1, the binding energies between copper and these monolayers should be negative. Negative binding energies that are large in magnitude indicate that copper and the monolayer have formed a strong bond and a stable structure. Moreover, referring to Equation 2, the presence of charge transfer is also an indicator of increased bond strength.

1.3.1 Copper-Boron Nitride

Copper coordination to boron nitride was performed using a 2×2 supercell with a kinetic energy cutoff of 24 Ha. Four binding locations (the top of the boron atom, the top of the nitrogen atom, the hollow of the monolayer, and the bridge site) were used to determine the most optimal binding site. All four of these binding locations demonstrated different binding affinities, and copper revealed a preference for the top of the boron atom. When copper is placed on top of the boron atom, this results in a binding energy of -0.5027 Ha which means that copper forms a stable structure with boron nitride. The site with the lowest binding affinity was the hollow site with a binding energy of -0.4419 Ha. Although less stable than the top of the boron atom, this binding site still results in a negative binding energy which shows that it forms a somewhat stable bond with the monolayer. Visualizations of the binding sites of boron nitride and copper as well as their charge transfers are shown in Figure 4. The binding energies are shown in Table V.

Table 5. *Binding Energies (Ha) for Copper Absorbed onto Boron Nitride. Cu^H , Cu^{TB} , Cu^{TN}, and Cu^B are representative of copper coordination to the center, top of the boron, top of the nitrogen, and bridge locations respectively*

Boron Nitride Copper Binding Configuration	$E_{binding}$ (Ha)
Cu^H	-0.4419
Cu^{TB}	-0.5027
Cu^{TN}	-0.5027
Cu^B	-0.5027

1.3.2 Copper-MoS_2

Similar to the copper and boron nitride calculations, copper coordination to MoS_2 was performed using a 2×2 supercell with a kinetic energy cutoff of 22 Ha. Three binding locations (the top of the Mo atom, the top of the S atom, and the hollow of the monolayer) were used to determine the most optimal binding site. Copper revealed a preference for the top of the Mo atom with a binding energy of -0.5417 Ha, which means that it forms a stable bond with the Mo atom. The site with the lowest binding affinity was the top of the S atom which had a binding energy of -0.5270 Ha. Although this binding energy is still negative, it is lower compared to the other binding sites and results in the least stable copper-MoS_2 structure. Visualizations of the binding sites of MoS_2 and copper and their charge transfers are shown in Figure 5. The binding energies are listed in Table VI.

Table 6. *Binding Energies (Ha) for Copper Absorbed onto the MoS_2 Surface. Cu^H, Cu^{TM}, and Cu^{TS} are representative of copper coordination to the center, top of the Mo atom, and top of the S atom, respectively*

MoS_2 Copper Binding Configuration	$E_{binding}$ (Ha)
Cu^H	-0.5368
Cu^{TM}	-0.5417
Cu^{TS}	-0.5270

1.3.3 Copper-Silicene

We also investigated copper coordination to the silicene surface using a 2×2 supercell, consistent with the previous calculations, and a kinetic energy cutoff of 22 Ha. We used three binding sites (the top of the Si

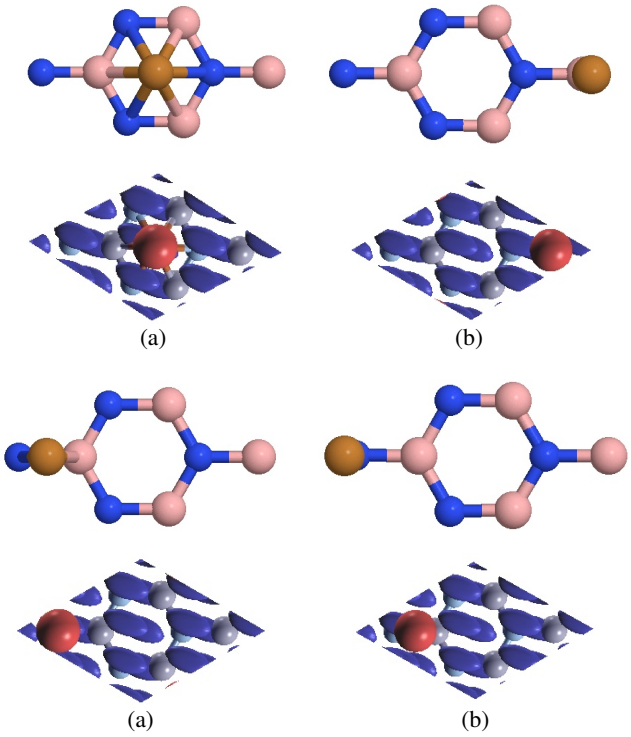

Figure 4. *The atomic structures of copper coordination to boron nitride followed by the charge transfers below. (a) The hollow of boron nitride, (b) The top of boron, (c) The top of nitrogen, and (d) The bridge site. For the atomic structures, the boron atoms are represented by pink, the nitrogen atoms by blue, and the copper atoms by brown. For the charge transfer, red shows the gain of negative charge, whereas blue shows the loss of negative charge. The isosurface value used was 0.03 e/Bohr^3*

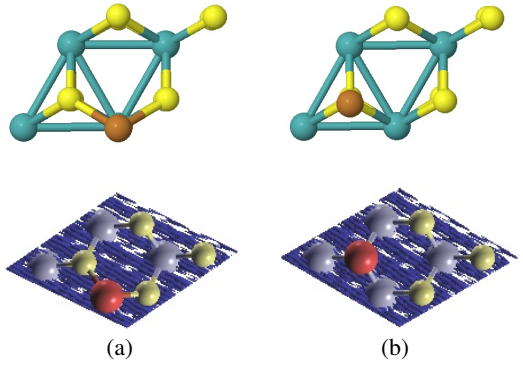

Figure 5. *The atomic structures of copper coordination to MoS_2 followed by the charge transfers below. (a) The top of the Mo atom and (b) The top of the S atom. For the atomic structures, the molybdenum atoms are represented by light blue, the sulfur atoms by yellow, and the copper atoms by brown. For the charge transfer, red shows the gain of negative charge, whereas blue shows the loss of negative charge. The isosurface value used was 0.03 e/Bohr^3*

atom, the hollow of the monolayer, and the bridge site) to find the most optimal binding site for silicene. Copper revealed a preference for the hollow site with a binding energy of -0.6298 Ha. This binding energy is the highest in magnitude compared to all of the copper-monolayer calculations which indicates that copper and the hollow of silicene form the most stable structure. The site with the lowest binding affinity was the bridge site with a binding energy of -0.5672 Ha. This binding energy is still significantly higher

PeerJ Preprints NOT PEER-REVIEWED

than some of the other copper-monolayer binding energies proving this configuration to be a relatively stable structure. Visualizations of the binding sites of silicene and copper as well as their charge transfers are shown in Figure 6. The binding energies are presented in Table VII.

Table 7. *Binding Energies (Ha) for Copper Absorbed onto the Silicene Surface. Cu^H, Cu^T, and Cu^B are representative of copper coordination to the center, top of the Si atom, and the bridge site, respectively*

Silicene Copper Binding Configuration	$E_{binding}$ (Ha)
Cu^H	-0.6298
Cu^T	-0.5809
Cu^B	-0.5672

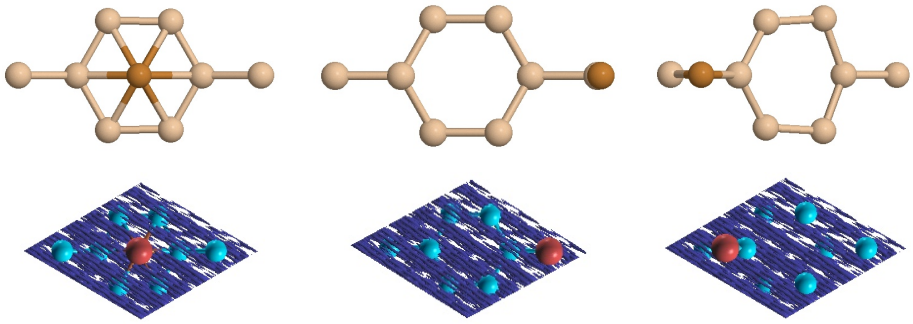

(a) (b) (c)

Figure 6. *Copper coordination to silicene followed by the charge transfers below. (a) The hollow of silicene, (b) The top of Si atom, and (c) The bridge site. For the atomic structures, the silicon atoms are represented by ivory and the copper atoms by brown. For the charge transfer, red shows the gain of negative charge, whereas blue shows the loss of negative charge. The isosurface value used was 0.03 e/Bohr^3*

Exploring the atomic structures and binding energies of copper to these three monolayers, we can see that copper forms stable structures with these three monolayers. Moreover, the presence of charge transfer between copper and the monolayers indiciates that it forms stable bonds. In charge transfer, the copper atom is seen gaining charge, whereas the monolayers are seen losing charge. More specifically, the gaining of charge occurs at the bonds between copper and the monolayer which demonstrates increased bond strength.

2 DISCUSSION

After processing our results, we found certain aspects of our research that require further analysis. There were two findings from the results of our study: First, that metal-induced aggregation of the Aβ protein varies due to pH changes and that in both high-pH and low-pH environments, copper truly has the highest affinity out of all metals for the Aβ binding site. Second, while the 2D materials investigated in this study don't directly have potential as metal chelators, their structural features and behavior when binding to copper (especially silicene) can spark further research in the field of AD related metal chelation.

2.1 Metal Interaction with Aβ

The total energy calculations and the binding energy calculations presented in this study revealed that the metal with the highest binding affinity to the Aβ protein was copper, followed by aluminum and zinc, respectively. While the metal-Aβ interaction affinities follow the same order at both the low-pH and the high-pH structures, values were observed to be consistently higher within the high pH coordination sphere. This is an important finding because the pH of the mammalian neuron lies between 7.03 and 7.46 (Ruffin et al. (2014)), making it ideal for Aβ aggregation.

During our investigation of metal binding to the first coordination sphere of the Aβ protein, we found that copper possessed the highest binding affinity in both the low-pH and the high-pH environments.

This result was expected since the first coordination sphere used in this study was derived from a Cu-Aβ structure, and therefore correlates with previous studies (Pavelka et al. (2006); Alí-Torres et al. (2015)). Moreover, copper as the metal ion with the highest binding affinity proposes that copper would be difficult to displace by other metals abundant in the brain. We can also hypothesize that this coordination sphere along the Aβ residue is the ideal location for copper-Aβ interaction.

The replacement of zinc as the central metal ion in the coordination complex resulted in the lowestbinding energy in context of this study. Previous studies examining zinc's coordination to the Aβ protein report that zinc ions form more flexible and open-coordinated geometries with the Aβ protein, promoting a higher amount of Aβ aggregation (Minicozzi et al. (2008a)). Another possible reason for the weak interaction between zinc and the structure used in this study can be the coordination number of the zinc-Aβ complex. With an ideal coordination from four histidine (abbreviated to His) ligands with the addition of an oxygen atom, zinc is reported to have a coordination number of five (Rana and Sharma (2019)) and presence of only four in the structures presently examined may also demonstrate zinc's low preference for this Aβ residue. The weak interactions reported in this study may also be a potential indication of zinc's high dependence on nitrogen containing groups, as the oxygen containing ligand is uncharacteristic of zinc's first coordination sphere. Future studies should explore zinc's coordination to different amino acid residues along the Aβ protein.

Aluminum, another metal used in this study, demonstrated a strong binding affinity to the Aβ protein. Due to its hard Lewis structure (Mujika et al. (2017)), aluminum prefers ligands that donate electrons, particularly oxygen-containing ligands. This varies from zinc and copper who both prefer nitrogen containing groups. In previous aluminum-Aβ coordination studies, it was found that along with oxygen containing ligands, aluminum also preferred carboxyl group ligands. This preference is further demonstrated through its predicted binding sites to consist of Glu3, Asp7, and Glu11 (Mujika et al. (2017)). It was found that the three carboxyl groups of the Glu3, Asp7, and Glu11 contributed the most stable aluminium-Aβ coordination sphere. The presence of oxygen in the structures used in this study, in both the low-pH and high-pH coordination spheres, may have contributed to aluminum's high binding energies. Future investigations regarding aluminum and Aβ should be carried out with a different site of ligands, such as Glu and Asp rather than His.

2.2 Metal Interaction with 2D Monolayer

During the course of this study, we investigated the binding of copper to three different materials: boron nitride, molybdenum disulfide, and silicene.

Boron nitride was chosen in this study due to its recent applications in biomedical settings. Boron nitride nanotubes have been used in the drug-delivery and treatment of brain diseases (Ciofani et al. (2011)) which makes the boron nitride monolayer a novel device for metal chelation. Moreover, the structure of boron nitride closely resembles graphene which has been proven to have promising results in the treatment of AD. Comparison of binding energies observed for copper coordination to the boron nitride surface at different locations indicated a preference for the top of the boron atom. The binding energy of the copper adsorbed boron nitride structure, despite demonstrating moderate affinity, was less than the binding energies of the copper-Aβ complexes with a value of -0.5027 Ha compared to -0.7262 Ha (high-pH) and -0.6842 (low-pH). However, the absolute differences between the binding energies of the copper-Aβ complexes and the copper-boron-nitride complex are 0.1815 Ha and 0.2235 Ha for the low-pH and high-pH scenarios, respectively. These minimal energy differences may prompt further research into boron nitride chelators with slight modifications, such as changes in pressure or temperature in order to develop a more effective material.

Binding energies between copper and molybdenum disulfide, proved similar inabilities towards direct chelation potential. Greatest preference was displayed for the site above the molybdenum atom, most likely due to this position's interaction with the nearby sulfur atoms. However, the binding energy was lower than that of the copper-Aβ complex, demonstrating this version of the material's inability to participate in copper chelation. This could be explained by the stability of molybdenum disulfide, as certain structures of molybdenum disulfide are less stable than others (Dallavalle et al. (2012)). Furthermore, the absolute differences between the binding energies of the copper-Aβ complexes and the copper-molybdenum-disulfide complexes are 0.1425 Ha and 0.1845 Ha or the low-pH and high-pH scenarios, respectively, proving that molybdenum disulfide may have potential as a chelator after slight modifications. Future studies should explore the different structures of molybdenum disulfide , both trigonal prismatic and

octahedral, as well as changes in pressure and temperature in order to yield the ideal monolayer for metal chelation.

Binding energies were also observed for copper coordination to the silicene material. Copper presented different binding affinities to different areas of the monolayer with a preference for the hollow site. Silicene was initially selected as its high surface area is suitable for metal adsorption, and its buckled structure points towards reactivity that may allow copper binding. Recent clinical trials have also revealed that silica particles may reduce the cognitive impairment associated with AD (Davenward et al. (2013)). Analysis of copper coordination to silicene revealed that copper displayed a preference for the hollow site. However, the binding energy at this site, was less than the copper-Aβ complex with a value of -0.6298 Ha compared to -0.6842 Ha (low-pH) -0.7262 Ha (high-pH). However, the absolute differences between the hollow configuration of silicene and the low- and high-pH copper-Aβ structures are 0.0544 Ha and 0.0964 Ha. These very minimal energy differences strongly correlate to the idea that silicene should be further explored in AD therapy. Future works should investigate environmental changes on the binding energies of silicene in order to produce an ideal chelator.

3 CONCLUSION

In summary, we performed Density Functional Theory calculations to determine the binding affinities between copper, zinc, aluminum, and the Aβ first coordination sphere as well as the binding affinities between copper, boron nitride, molybdenum disulfide, and silicene. For the metal-Aβ complexes, we substituted a series of metal ions with biological significance in the first coordination sphere estimated for copper-Aβ binding. Investigation of the binding energies of the different metals to the coordination sphere confirmed that copper retained the strongest affinity. Both low-pH and high-pH environments were considered, and the investigation revealed that the metal-Aβ complexes preferred the high-pH environment. These findings are expected to increase the research community's understanding of copper, aluminum, and zinc metal ions' interaction with the Aβ ligand in Alzheimer's disease.

Binding energy calculations and charge transfer calculations were conducted for the copper-2D monolayer structures. The direct chelation potential of these monolayers was determined by comparing the copper-2D monolayer binding energies to the binding energy of the copper-Aβ complexes in both the low-pH and the high-pH environments. Examining our results, we found that the monolayer that produced the highest binding energy was silicene when copper was coordinated to its hollow site. Even though the binding energy was less than the copper-Aβ complexes, the absolute differences between the hollow configuration of silicene and the low- and high-pH copper-Aβ structures were 0.0544 Ha and 0.0964 Ha, proving further research into silicene a valuable task. The same conclusion applies for boron nitride and molybdenum disulfide as well. Further research into these monolayers as well as the manipulation of internal and external properties will pave the way for chelation therapy in Alzheimer's disease.

Investigations in this study significantly contribute to the understanding of Alzheimer's disease and the mechanical roles metal ions play in its progression; however, the platforms implemented in this study are limited to only the first coordination sphere of the Aβ protein. Future explorations in this field may consider the continuation of these computational approaches on the full length Aβ model to allow consideration of physical effects of the rest of the sequence. Works aiming to develop upon this study may also expand upon the variation in the valence states or the coordination numbers in order to develop a deeper exploration. Because the application of 2D materials as chelating agents is a new field in the development of Alzheimer's therapy, many monolayers and their effects on the metals relevant to AD progression are largely unexplored. This study has identified the role of biologically significant metals in Aβ aggregation and has identified promising metal chelators for future research.

ACKNOWLEDGMENTS

We would like to thank Dr. Geifei Qian for the technical assistance.

REFERENCES

Alí-Torres, J., Mirats, A., Maréchal, J.-D., Rodríguez-Santiago, L., and Sodupe, M. (2015). Modeling cu2+-aβ complexes from computational approaches. *AIP Advances*, 5(9):092402.

Azimi, S. and Rauk, A. (2011). On the involvement of copper binding to the n-terminus of the amyloid beta peptide of alzheimer's disease: a computational study on model systems. *International Journal of Alzheimer's Disease*, 2011.

Barnham, K. J. and Bush, A. I. (2014). Biological metals and metal-targeting compounds in major neurodegenerative diseases. *Chemical Society Reviews*, 43(19):6727–6749.

Barnham, K. J., Curtain, C. C., and Bush, A. I. (2007). Free radicals, metal ions, and aβ aggregation and neurotoxicity. In *Protein Misfolding, Aggregation, and Conformational Diseases*, pages 31–47. Springer.

Blöchl, P. E. (1994). Projector augmented-wave method. *Physical review B*, 50(24):17953.

Cheng, Y., Feng, Z., Zhang, Q.-z., and Zhang, J.-t. (2006). Beneficial effects of melatonin in experimental models of alzheimer disease. *Acta Pharmacologica Sinica*, 27(2):129.

Ciofani, G., Danti, S., Ricotti, L., D'Alessandro, D., Moscato, S., Berrettini, S., Mattoli, V., and Menciassi, A. (2011). Boron nitride nanotubes: production, properties, biological interactions and potential applications as therapeutic agents in brain diseases. *Current Nanoscience*, 7(1):94–109.

Curtain, C. C., Ali, F., Volitakis, I., Cherny, R. A., Norton, R. S., Beyreuther, K., Barrow, C. J., Masters, C. L., Bush, A. I., and Barnham, K. J. (2001). Alzheimer's disease amyloid-β binds copper and zinc to generate an allosterically ordered membrane-penetrating structure containing superoxide dismutase-like subunits. *Journal of Biological Chemistry*, 276(23):20466–20473.

Dallavalle, M., Sandig, N., and Zerbetto, F. (2012). Stability, dynamics, and lubrication of mos2 platelets and nanotubes. *Langmuir*, 28(19):7393–7400.

Datta, A., Ramamurty, U., Ranganathan, S., and Waghmare, U. (2006). Crystal structures of a mg–zn–y alloy: A first-principles study. *Computational Materials Science*, 37(1-2):69–73.

Davenward, S., Bentham, P., Wright, J., Crome, P., Job, D., Polwart, A., and Exley, C. (2013). Silicon-rich mineral water as a non-invasive test of the 'aluminum hypothesis' in alzheimer's disease. *Journal of Alzheimer's Disease*, 33(2):423–430.

Davey, W. P. (1925). Precision measurements of the lattice constants of twelve common metals. *Physical Review*, 25(6):753.

DeKosky, S. T. and Scheff, S. W. (1990). Synapse loss in frontal cortex biopsies in alzheimer's disease: correlation with cognitive severity. *Annals of Neurology: Official Journal of the American Neurological Association and the Child Neurology Society*, 27(5):457–464.

Dickson, D. W., Farlo, J., Davies, P., Crystal, H., Fuld, P., and Yen, S.-H. (1988). Alzheimer's disease. a double-labeling immunohistochemical study of senile plaques. *The American Journal of Pathology*, 132(1):86.

Drew, S. C., Noble, C. J., Masters, C. L., Hanson, G. R., and Barnham, K. J. (2009). Pleomorphic copper coordination by alzheimer's disease amyloid-β peptide. *Journal of the American Chemical Society*, 131(3):1195–1207.

Faller, P., Hureau, C., and Berthoumieu, O. (2013). Role of metal ions in the self-assembly of the alzheimer's amyloid-β peptide. *Inorganic Chemistry*, 52(21):12193–12206.

Gomez-Castro, C. Z., Vela, A., Quintanar, L., Grande-Aztatzi, R., Mineva, T., and Goursot, A. (2014). Insights into the oxygen-based ligand of the low ph component of the cu2+-amyloid-β complex. *The Journal of Physical Chemistry B*, 118(34):10052–10064.

Gonze, X., Amadon, B., Anglade, P.-M., Beuken, J.-M., Bottin, F., Boulanger, P., Bruneval, F., Caliste, D., Caracas, R., Cote, M., Deutsch, T., Genovese, L., Ghosez, P., Giantomassi, M., Goedecker, S., Hamann, D., Hermet, P., Jollet, F., Jomard, G., Leroux, S., Mancini, M., Mazevet, S., Oliveira, M., Onida, G., Pouillon, Y., Rangel, T., Rignanese, G.-M., Sangalli, D., Shaltaf, R., Torrent, M., Verstraete, M., Zerah, G., and Zwanziger (2009). Abinit: First-principles approach of materials and nanosystem properties. *Computer Physics Communications*, 180:2582–2615.

Han, Q., Cai, S., Yang, L., Wang, X., Qi, C., Yang, R., and Wang, C. (2017). Molybdenum disulfide nanoparticles as multifunctional inhibitors against alzheimer's disease. *ACS Applied Materials & Interfaces*, 9(25):21116–21123.

Hane, F., Tran, G., Attwood, S. J., and Leonenko, Z. (2013). Cu2+ affects amyloid-β (1–42) aggregation by increasing peptide-peptide binding forces. *PloS One*, 8(3):e59005.

Hardy, J. A. and Higgins, G. A. (1992). Alzheimer's disease: the amyloid cascade hypothesis. *Science*, 256(5054):184–186.

Karr, J. W. and Szalai, V. A. (2007). Role of aspartate-1 in cu (ii) binding to the amyloid-β peptide of

alzheimer's disease. *Journal of the American Chemical Society*, 129(13):3796–3797.

Kowalik-Jankowska, T., Ruta, M., Wiśniewska, K., and Łankiewicz, L. (2003). Coordination abilities of the 1–16 and 1–28 fragments of β-amyloid peptide towards copper (ii) ions: a combined potentiometric and spectroscopic study. *Journal of Inorganic Biochemistry*, 95(4):270–282.

Lannfelt, L., Blennow, K., Zetterberg, H., Batsman, S., Ames, D., Harrison, J., Masters, C. L., Targum, S., Bush, A. I., Murdoch, R., et al. (2008). Safety, efficacy, and biomarker findings of pbt2 in targeting aβ as a modifying therapy for alzheimer's disease: a phase iia, double-blind, randomised, placebo-controlled trial. *The Lancet Neurology*, 7(9):779–786.

Lee, M., Kim, J. I., Na, S., and Eom, K. (2018). Metal ions affect the formation and stability of amyloid β aggregates at multiple length scales. *Physical Chemistry Chemical Physics*, 20(13):8951–8961.

Lesné, S., Koh, M. T., Kotilinek, L., Kayed, R., Glabe, C. G., Yang, A., Gallagher, M., and Ashe, K. H. (2006). A specific amyloid-β protein assembly in the brain impairs memory. *Nature*, 440(7082):352.

Liu, G., Men, P., Perry, G., and Smith, M. A. (2009). Metal chelators coupled with nanoparticles as potential therapeutic agents for alzheimer's disease. *Journal of nanoneuroscience*, 1(1):42–55.

Mantsyzov, A. B., Savelyev, O. Y., Ivantcova, P. M., Bräse, S., Kudryavtsev, K. V., and Polshakov, V. I. (2018). Theoretical and nmr conformational studies of β-proline oligopeptides with alternating chirality of pyrrolidine units. *Frontiers in Chemistry*, 6:91.

Marino, T., Russo, N., Toscano, M., and Pavelka, M. (2010). On the metal ion (zn 2+, cu 2+) coordination with beta-amyloid peptide: Dft computational study. *Interdisciplinary Sciences: Computational Life Sciences*, 2(1):57–69.

Minicozzi, V., Morante, S., Rossi, G., Stellato, F., Christian, N., and Jansen, K. (2008a). The role of metals in amyloid aggregation—experiments and ab initio simulations. *International Journal of Quantum Chemistry*, 108(11):1992–2015.

Minicozzi, V., Stellato, F., Comai, M., Dalla Serra, M., Potrich, C., Meyer-Klaucke, W., and Morante, S. (2008b). Identifying the minimal copper-and zinc-binding site sequence in amyloid-β peptides. *Journal of Biological Chemistry*, 283(16):10784–10792.

Molina-Sanchez, A. and Wirtz, L. (2011). Phonons in single-layer and few-layer mos 2 and ws 2. *Physical Review B*, 84(15):155413.

Mujika, J. I., Pedregal, J. R.-G., Lopez, X., Ugalde, J. M., Rodríguez-Santiago, L., Sodupe, M., and Maréchal, J.-D. (2017). Elucidating the 3d structures of al (iii)–aβ complexes: a template free strategy based on the pre-organization hypothesis. *Chemical Science*, 8(7):5041–5049.

Mutter, S. T., Deeth, R. J., Turner, M., and Platts, J. A. (2018). Benchmarking of copper (ii) lfmm parameters for studying amyloid-β peptides. *Journal of Biomolecular Structure and Dynamics*, 36(5):1145–1153.

Pappolla, M., Bozner, P., Soto, C., Shao, H., Robakis, N. K., Zagorski, M., Frangione, B., and Ghiso, J. (1998). Inhibition of alzheimer β-fibrillogenesis by melatonin. *Journal of Biological Chemistry*, 273(13):7185–7188.

Pavelka, M., Šimánek, M., Šponer, J., and Burda, J. V. (2006). Copper cation interactions with biologically essential types of ligands: A computational dft study. *The Journal of Physical Chemistry A*, 110(14):4795–4809.

Perdew, J. P., Burke, K., and Ernzerhof, M. (1996). Generalized gradient approximation made simple. *Physical review letters*, 77(18):3865.

Pflugradt, P., Matthes, L., and Bechstedt, F. (2014). Silicene on metal and metallized surfaces: ab initio studies. *New Journal of Physics*, 16(7):075004.

Rana, M. and Sharma, A. K. (2019). Cu and zn interactions with aβ peptides: Consequence of coordination on aggregation and formation of neurotoxic soluble aβ oligomers. *Metallomics*, 11(1):64–84.

Rauk, A. (2009). The chemistry of alzheimer's disease. *Chemical Society Reviews*, 38(9):2698–2715.

Riley, K. P., Snowdon, D. A., and Markesbery, W. R. (2002). Alzheimer's neurofibrillary pathology and the spectrum of cognitive function: findings from the nun study. *Annals of Neurology*, 51(5):567–577.

Rimola, A., Alí-Torres, J., Rodríguez-Rodríguez, C., Poater, J., Matito, E., Sola, M., and Sodupe, M. (2011). Ab initio design of chelating ligands relevant to alzheimer's disease: Influence of metalloaromaticity. *The Journal of Physical Chemistry A*, 115(45):12659–12666.

Ritchie, C. W., Bush, A. I., Mackinnon, A., Macfarlane, S., Mastwyk, M., MacGregor, L., Kiers, L., Cherny, R., Li, Q.-X., Tammer, A., et al. (2003). Metal-protein attenuation with iodochlorhydroxyquin (clioquinol) targeting aβ amyloid deposition and toxicity in alzheimer disease: a pilot phase 2 clinical

trial. *Archives of Neurology*, 60(12):1685–1691.

Ruffin, V. A., Salameh, A. I., Boron, W. F., and Parker, M. D. (2014). Intracellular ph regulation by acid-base transporters in mammalian neurons. *Frontiers in Physiology*, 5:43.

Selkoe, D. J. (2001). Alzheimer's disease: genes, proteins, and therapy. *Physiological Reviews*, 81(2):741–766.

Smith, D. G., Cappai, R., and Barnham, K. J. (2007). The redox chemistry of the alzheimer's disease amyloid β peptide. *Biochimica et Biophysica Acta (BBA)-Biomembranes*, 1768(8):1976–1990.

Strodel, B. and Coskuner-Weber, O. (2019). Transition metal ion interactions with disordered amyloid-β peptides in the pathogenesis of alzheimer's disease: Insights from computational chemistry studies. *Journal of Chemical Information and Modeling*, 59(5):1782–1805.

Syme, C. D., Nadal, R. C., Rigby, S. E., and Viles, J. H. (2004). Copper binding to the amyloid-β (aβ) peptide associated with alzheimer's disease folding, coordination geometry, ph dependence, stoichiometry, and affinity of aβ-(1–28): Insights from a range of complementary spectroscopic techniques. *Journal of Biological Chemistry*, 279(18):18169–18177.

Talley, J. M., Cerda, B. A., Ohanessian, G., and Wesdemiotis, C. (2002). Alkali metal ion binding to amino acids versus their methyl esters: Affinity trends and structural changes in the gas phase. *Chemistry–A European Journal*, 8(6):1377–1388.

Tanzi, R. E., Gusella, J. F., Watkins, P. C., Bruns, G., St George-Hyslop, P., Van Keuren, M. L., Patterson, D., Pagan, S., Kurnit, D. M., and Neve, R. L. (1987). Amyloid beta protein gene: cdna, mrna distribution, and genetic linkage near the alzheimer locus. *Science*, 235(4791):880–884.

Tõugu, V., Tiiman, A., and Palumaa, P. (2011). Interactions of zn (ii) and cu (ii) ions with alzheimer's amyloid-beta peptide. metal ion binding, contribution to fibrillization and toxicity. *Metallomics*, 3(3):250–261.

Viles, J. H. (2012). Metal ions and amyloid fiber formation in neurodegenerative diseases. copper, zinc and iron in alzheimer's, parkinson's and prion diseases. *Coordination Chemistry Reviews*, 256(19-20):2271–2284.

Wang, J., Ma, F., and Sun, M. (2017). Graphene, hexagonal boron nitride, and their heterostructures: properties and applications. *RSC Advances*, 7(27):16801–16822.